Computer Assisted Mechanics and Engineering Sciences, 7: 91–101, 2000.

Finite element analysis and experimental investigations of the intervertebral disc in the human lumbar, cervical spine and porcine lumbar spinal segment

Michał Ciach and Jan Awrejcewicz
Division of Automatics and Biomechanics, Faculty of Mechanical Engineering, Technical University of Łódź, Stefanowskiego 1/15, 90-924 Łódź, Poland

(Received April 13, 1999)

The main objective of this study is to design three-dimensional geometrical and mechanical finite element model of the intervertebral disc between L2–L3 vertebras in the lumbar and C5–C6 cervical spinal segment. The model was directed toward understanding the work and the role of the intervertebral disc that performs in the human spinal segment body. The three-dimensional finite element motion segment was developed and its response to different loads was performed. The model accounted for the solid component of the nucleus pulposus while anulus fibrosus was modeled as a matrix of homogeneous ground substance reinforced by anulus fibers. End plates similarly to the nucleus pulposus were simulated using volumic elements. Simultaneously the vertebral bodies have been modeled as a complex construction of a cancellous core covered by a cortical shell of the orthotropic material properties. Isotropic material has been used to model posterior elements. To simulate ligament like behavior, tension only elements have been used. Numerical studies of the lumbar segment have been consequently compared with the experimental investigation performed on the porcine model by authors and other in vitro experiments on human lumbar spine accomplished by other scientists. In cervical spinal segment numerically two surgical techniques (Cloward and Robinson–Smith) have been tested. Two types of loads have been applied to three models – to an intact C5–C6 spinal segment and then to the vertebras after performing those two surgical techniques. All numerical analysis have been undertaken using ANSYS 5.4 commercial application.

1. Introduction

The spine is a non-homogeneous complex-shape construction of 24 vertebrae, separated by intervertebral discs with numerous muscles and ligaments attached to them. Intervertebral discs act as a kind of cushion to soften the impacts caused by the movement of body [1, 18]. The intervertebral discs make up about one fourth of entire length of the vertebral column. The discs absorb the stress and strain transmitted to the vertebral column. The intervertebral disc is a composite structure composed of the anulus fibrosus [2, 5, 10, 20], the nucleus pulposus [9] and the end plates. The anulus fibrosus is a collagen-fiber-reinforced composite angle play structure that surrounds the nucleus pulposus. It resists hoop stresses due to compressive loads and the bending and torsional stresses produced by everyday activities of bending and rotation. The fibers of the anulus form lamellae, or individual layers of parallel collagen fibers that attach to the superior and inferior end plates. The orientation of the individual lamellae alternates with successive layers between approximately $60°$ and $-60°$ to the vertical axis of the spine [2, 5, 10, 20]. Nucleus pulposus is the inner gelatinous (proteoglycan–laden gel), highly hydrated core. The gelatin nature of the nucleus pulposus constrained by the anulus ensures its high water content and cushioning properties [9]. The nucleus pulposus is located slightly posterior from the center of the intervertebral disc. The cartilaginous end plate of the spine is a thin layer of hyaline cartilage, which lines the interior, and superior surface of the vertebral body (Fig. 1). It consists primarily of collagen, proteoglycan and water. The end plate is centrally situated in the vertebral body, adjacent to the nucleus pulposus, and it has intimate attachments to the annulus fibrosus. The shape and dimension of a disc generally

corresponds to the shape of the end plates to which the disc is attached. Consequently the shapes of the discs depend on their location in the spinal column [1, 18].

2. The finite element model of the L2–L3 lumbar spine

A three dimensional finite element model of intact L2–L3 motion segment was created to study its behaviour under different loading condition using a commercially available finite element application, ANSYS 5.4. Mesh geometry was obtained from computer topographic scans for the shape and diameters of the intervertebral disc while the shape of vertebras was approximated by "in life" measurements of cadaveric spine [6, 7, 11–14, 16, 18]. The intact segment contained a total of 16904 nodes and 9132 elements.

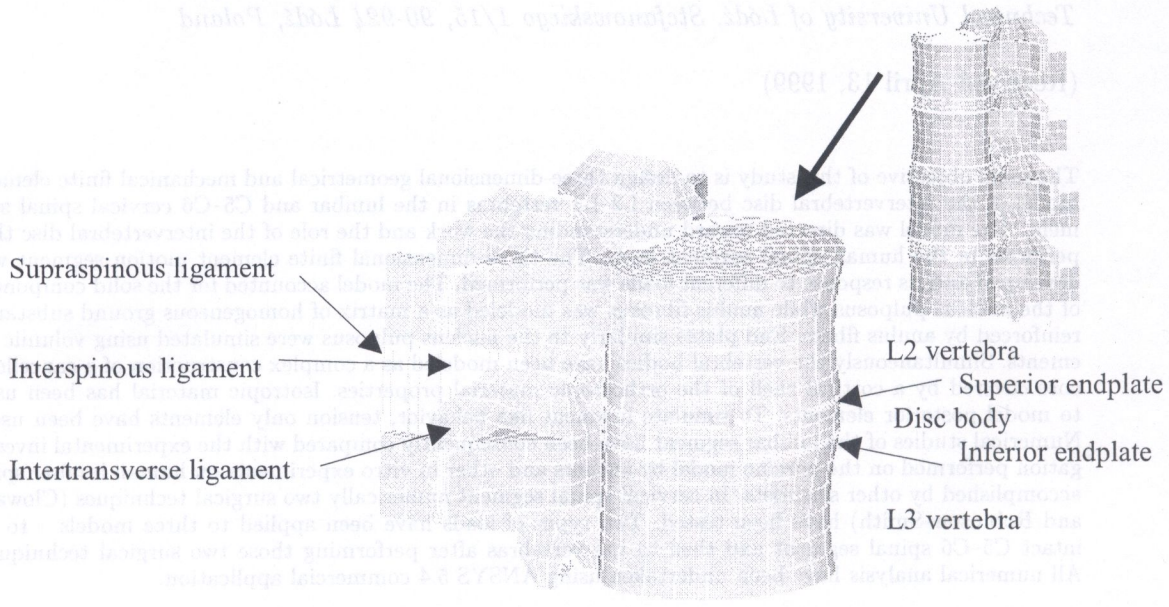

Fig. 1. Finite element mesh used for the purpose of the analysis of L2–intervertebral disc–L3 body units

The vertebral bodies have been modeled as a complex construction of a cancellous core covered by a cortical shell (2 mm thick). Cartilaginous end plates at the superior and inferior surfaces of the intervertebral discs were assumed to be 1 mm thick. The anulus fibrosus was modeled as a matrix of homogeneous ground substance reinforced by anulus fibers and consisted of five layers of elements going radially, three layers going vertically and 24 going circumferentially thus making it possible to model composite like structure of the disc. The collagenous fibers were represented by three-dimensional uniaxial tension only spar elements having the feature of a bilinear stiffness matrix, attached along diagonals of isotropic solid elements of anulus ground substance. The spar elements have three degrees of freedom at each node: translation in the nodal x, y, and z direction. For the elements no bending stiffness is included. Anulus fiber orientation varied from 19° (for the outer-most fibers) to 30° (for the innermost layers) to the end plates, which compares with results in the literature (Fig. 2) [2, 5, 6, 11–14, 20–21]. The posterior elements have been modeled using eight-node solid elements. They were reinforced with ligaments, which were constructed similarly to anulus fibers as tension only elements. The nucleus pulposus was assumed to be simulated as volumic elements with a Poisson coefficient of 0.499 representing a quasi-isovolumic bevaviour [10]. The disc cross-sectional area was 1313 mm2 and the ratio of nucleus pulposus to disc cross-sectional area was 39%, which is well in range of 30–50% given in the literature [5, 9, 11–14, 20]. For succeeding large deformation nonlinear numerical analysis has been performed. Cortical and cancellous bone were simulated using 3D eight-node solid volumic elements with three degrees of freedom at each node:

translation in the nodal x, y, and z direction. Orthotropic material properties have been assigned to the vertebral bodies. Their orthotropy has been modeled with a respect to the global coordinate system where z-axis was parallel to the longitudinal axis of the spine.

Table 1 shows the dimensions of the model.

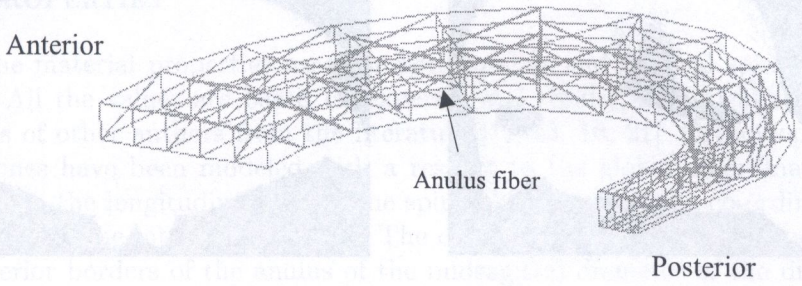

Fig. 2. Finite element model approximation of the intervertebral disc anulus fibers

Table 1. Geometry factors of the model

Disc height (mm)	8
Lateral disc diameter (mm)	47.5
Anterior–posterior disc diameter (mm)	32.7
Disc cross-sectional area (mm^2)	1312.9
Nucleus cross-sectional area (mm^2)	506.53
End plate thickness (mm)	1.00
Vertebra height (L2 and L3) (mm)	26
Anulus fibers orientation (°)	19–30
Ligaments (mm^2):	
Supraspinous (SSL)	30
Interspinous (ISL)	40
Intertransverse (ITL)	4
Anterior longitudinal ligament (ALL)	64
Posterior longitudinal ligament (PLL)	20

3. Finite element model of the cervical spine

Mesh geometry was obtained from computer tomographic scans for the shape and diameters of vertebras of the whole spine. Files containing geometry of the cervical spine have been translated to the form readable for ANSYS 5.4. Surfaces, volumes and element have been generated for the cervical vertebras respectively (Fig. 3) [7].

In order to reduce the time of the numerical analysis consequently the number of elements has been significantly decreased. To create a geometrical model of C3–C7 vertebras, a C6 vertebra has been constructed and copied with a proper scale factor and with a respect to human male lordotic cervical spine curvatures, which have been investigated by Harrison *et al.* [6]. The mean curvature of the human male spine has been assumed in the model (Table 2).

A three dimensional finite element model of intact C2–C7 motion segment was created to study its behaviour under different loading condition using ANSYS 5.4 [16–17].

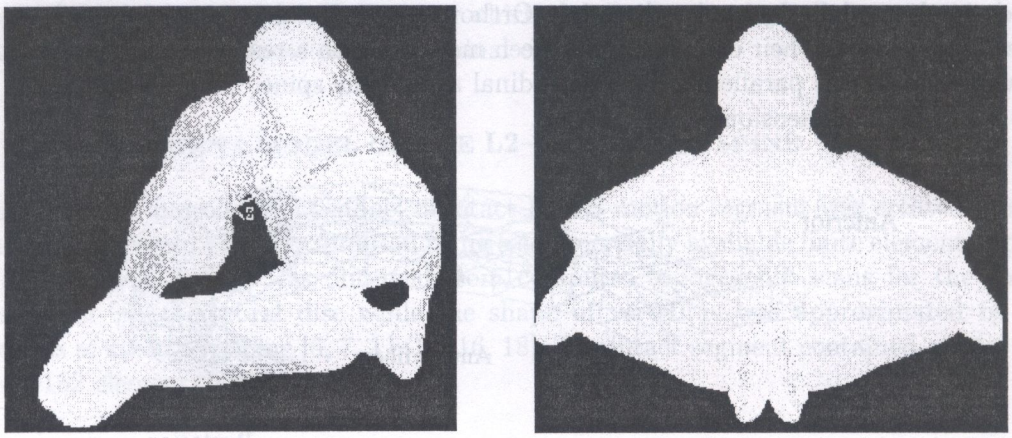

Fig. 3. An example of C2 (rotator) vertebra generated in the first stage of investigation

Table 2. Lordotic cervical spine curvatures (comparisons of 237 men and 163 women

	Mean	
Category	Males	Females
Age	34.04	37.42
Height/length (%)	96.95	97.02
Atlas angle (°)	23.23	25.22
Anterior translation (mm)	15.35	15.53
Absolute RA (C2–C7)	−34.32	−33.51
Relative RA (C2–C3)	−7.20	−8.69
Relative RA (C3–C4)	−6.01	−7.43
Relative RA (C4–C5)	−7.34	−6.90
Relative RA (C5–C6)	−6.46	−5.11
Relative RA (C6–C7)	−7.39	−5.42

RA = rotation angle

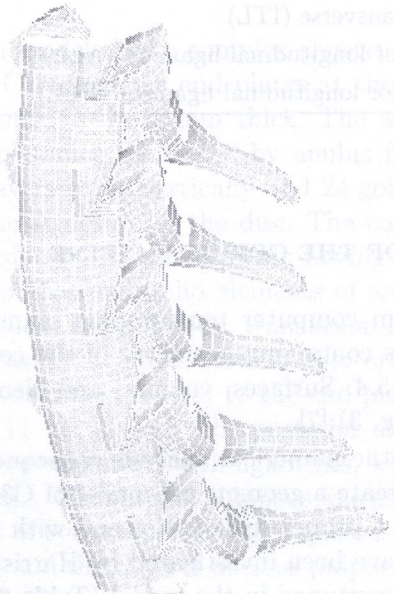

Fig. 4. Finite element mesh of C3–C7 vertebras

The vertebral bodies and the structure of the intervertebral discs have been modeled in the same way like for the lumbar spine, taking into account the shape and the size of the cervical spine, which was obtained from computer tomographic scans.

4. Material properties

In the Table 3, the material properties used for both lumbar and cervical spinal segment models have been listed. All the values are based on experimental results, analytical studies and former numerical analysis of other authors from the literature [11–13, 16, 21]. Orthotropy of the cortical and cancellous bones have been modeled with a respect to the global co-ordinate system where z-axis was parallel to the longitudinal axis of the spine. The origin of the co-ordinate stystem was located at the center of the intervertebral disc. The disc was located at the midpoint between the anterior and posterior borders of the anulus of the midsagittal diameter of the disc. At this stage of the project all material properties were assumed to be linear and their orthotropy were defined with respect to the global co-ordinate systems of the model (excluding anulus fibers which have their own co-ordinate systems). In a subsequent investigation hyperelastic material properties for anulus pulposus and viscoelastic properties for anulus fibers will be considered.

Table 3. Material properties applied to the model

Material	Young's modulus (MPa)	Poisson ratio
Cortical bone	$E_{xx} = E_{yy} = 13000$, $E_{zz} = 20000$, $G_{xy} = 3800$, $G_{xz} = G_{yz} = 5400$	$\nu_{xy} = \nu_{yx} = 0.484$, $\nu_{xz} = \nu_{yz} = 0.203$
Cancellous bone	$E_{xx} = E_{yy} = 140$, $E_{zz} = 200$, $G_{xy} = 48.3$, $G_{xz} = G_{yz} = 48.3$	$\nu_{xy} = \nu_{yx} = 0.45$, $\nu_{xz} = \nu_{yz} = 0.315$
Cartilaginous end-plates	$E = 23.8$	$\nu = 0.4$
Anulus ground substance	$E = 4.0$	$\nu = 0.4$
Anulus fibers	$E = 500.0$	$\nu = 0.35$
Nucleus pulposus	$E = 1.0$	$\nu = 0.499$
Ligaments:		
Supraspinous (SSL)	$E = 50$	$\nu = 0.35$
Interspinous (ISL)	$E = 50$	$\nu = 0.35$
Intertransverse (ITL)	$E = 150$	$\nu = 0.35$
Anterior longitudinal ligament (ALL)	$E = 20$	$\nu = 0.35$
Posterior longitudinal ligament (PLL)	$E = 40$	$\nu = 0.35$

5. Finite element model – boundary and loading conditions

Three types of numerical investigation of the lumbar spinal segment and two for the cervical spine have been accomplished. For lumbar spine axial compression, flexion–extension analysis and axial torque have been performed while for cervical spine only axial compression and flexural bending have been investigated. The inferior surface of the inferior vertebral body (L3/C6) has been fixed in all direction. For axial compression a load has been applied similarly to experiments as displacement attached to the nodes of the most anterior surface of the anterior vertebral body (L2/C5). The displacement was applied gradually with a factor of 0.1 mm. The adequate reaction has been calculated as a sum of reactions where the load had been applied. Moments – in flexion, extension and torsion have been consequently applied as pure moments to the nodes of the most anterior surface of the anterior vertebral body (L2/C5). The results of numerical investigation have been

compared with the experimental results from the literature [2, 5, 10, 17, 22] and with those, which were performed by authors on the porcine model.

6. Application of the model to the problem of cervical spine discectomy – two surgical operation techniques

In order to analyze two surgical techniques two finite element models have been constructed.

From medical point of view Cloward's technique involves hole drilling through a disc and adjacent vertebral bodies until posterior cortex is observed using a specially designed 12 mm drill bit. A disc and osteophyte are removed through a hole using curretes and other instruments. After completion of discectomy a dowel-shaped bone graft 1.5 mm wider than the hole is firmly tapped into place. The graft has a cortical layer at each end and cancellous bone in between.

In Robinson-Smith technique with traction applied to the cervical spine, only the intervertebral disc material and end plates of adjacent vertebral bodies are removed. Care is taken to ensure the presence of cancellous bone interface at the adjacent vertebral bodies. The created space usually accepts a block of bone graft 10–15 mm high, 10–15 mm wide and 10–15 mm deep. The graft has cortical layers and a cancellous bone. The graft is tapped in securely and countersunk in relation to the anterior cortical edges of the intervertebral aperture.

For the proposes of the analysis two different models have been constructed – one assuming the situation after performing Cloward operation techniques, another one taking into account condition of the spine after using Robinson–Smith operation technique. Material properties for cortical and cancellous bones were assumed to be the same like shown in the Table 3. Loading and boundary condition were applied in a same way like to an intact C5–C6 segment.

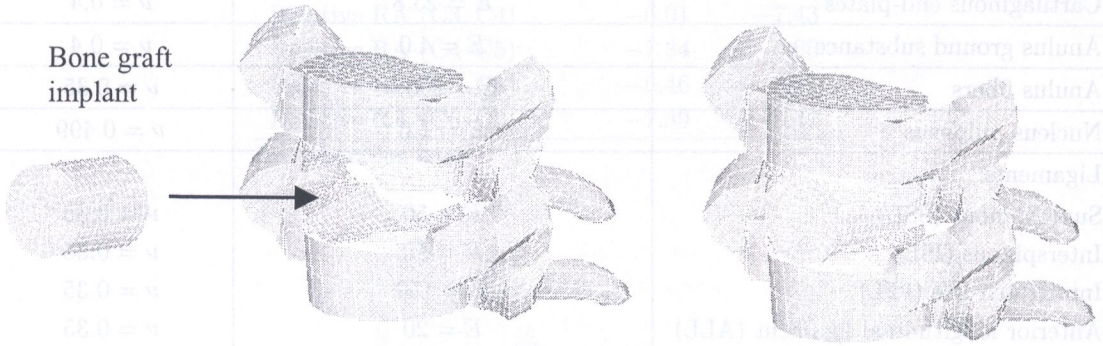

Fig. 5. Cloward surgery operation technique

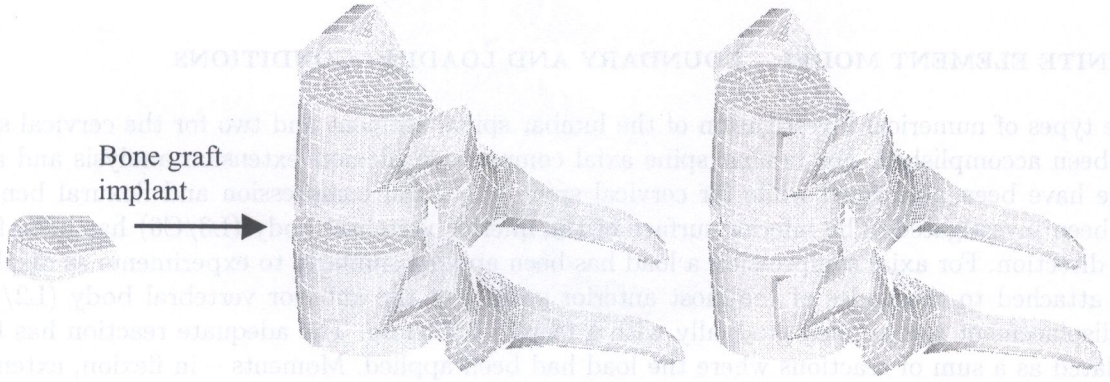

Fig. 6. Robinson–Smith surgery operation technique

7. Experimental investigation

Mechanical testing was performed on a porcine spine. L2–L3 vertebras have been taken into consideration. Before testing it was harvested, cleaned of all soft tissues while leaving all the ligamentous structures intact, and stored at $-20°C$. On the day of testing the specimen was thawed to room temperature and mounted. The inferior vertebral body (L3) has been fixed in all direction, while the most anterior surface of the anterior vertebral body (L2) has been attached to the top plate where different loads were being applied. Two extensometers have been attached to two vertebras (to the anterior and lateral part of L1–L2, respectively). Three types of experimental studies have been accomplished – axial compression, flexion–extension analysis and axial torque. In axial compression axial load was applied to the top plate clamped to the anterior surface of the anterior vertebral body. Special load gauges designed for the purposes of the investigation measured loads applied to the plate. Loads in flexion–extension states were applied like shown in Fig. 7, while pure torsion moments were used to investigate behavior of specimen in axial torque state. In axial compression and flexion–extension tests displacement–rotation was measured using extensometers while in axial torque displacement was measured using micrometer. Figure 7 displays all three methods of applying loads to the model.

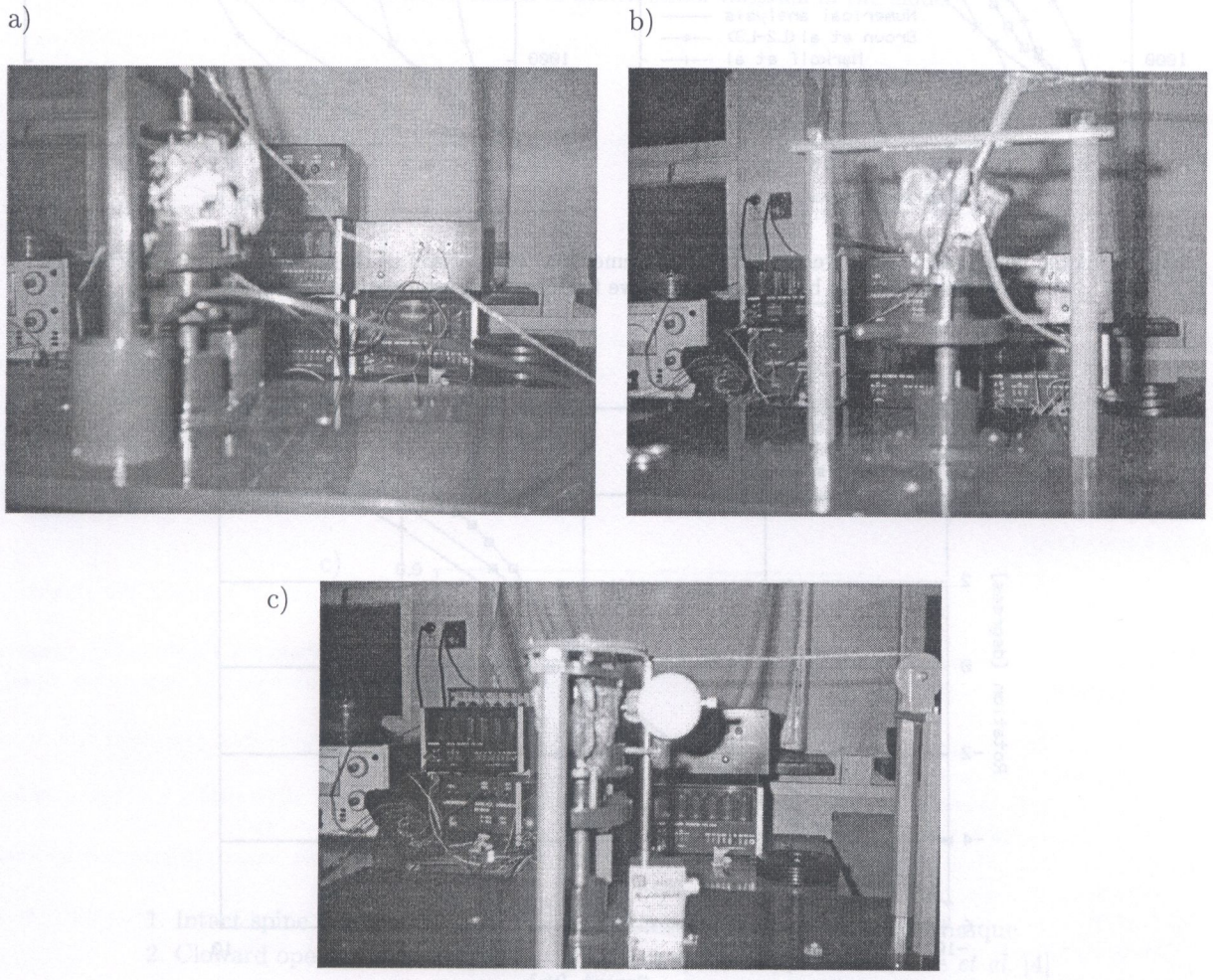

Fig. 7. Experimental study of the porcine model: a) axial compression, b) flexion–extension, c) axial torque

8. Results

Graphs in Figs. 8 and 9 display the behavior of the human and porcine lumbar segment models in axial compression, flexion–extension and axial torque states, respectively. Numerical and experimental analysis are compared showing significant correspondence of both numerical and experimental investigations.

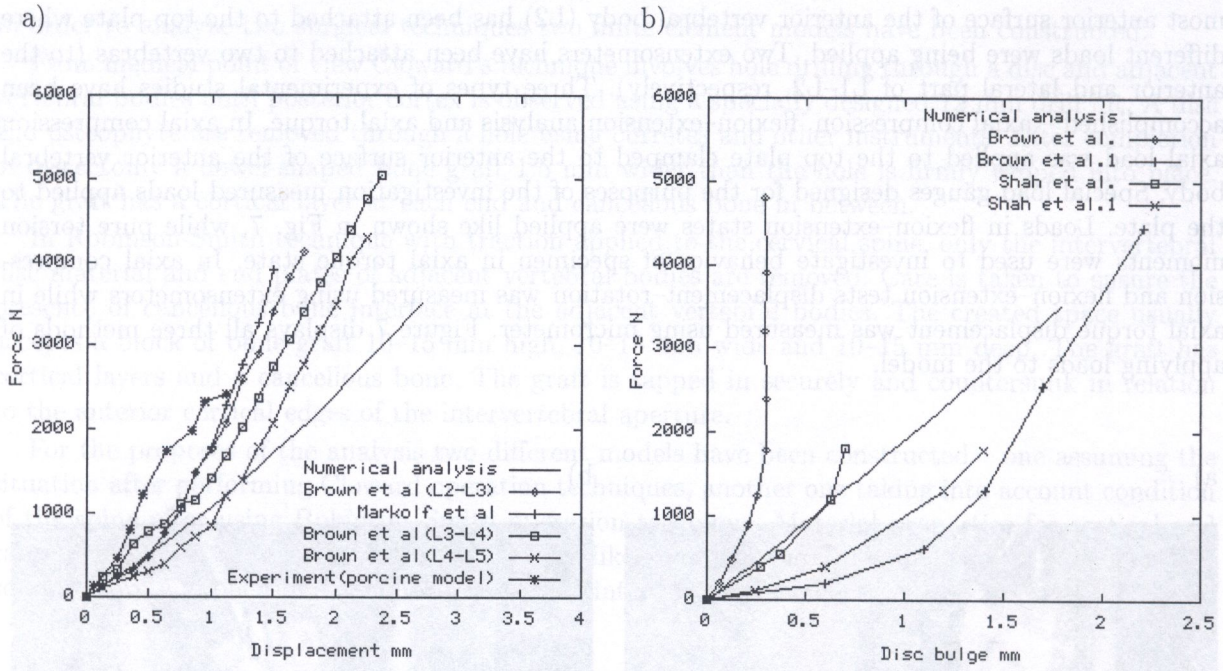

Fig. 8. Axial compressive force versus axial displacement; a) comparison of the numerical and experimental results [3, 15, 19] b) axial compressive force versus posterolateral disc bulge

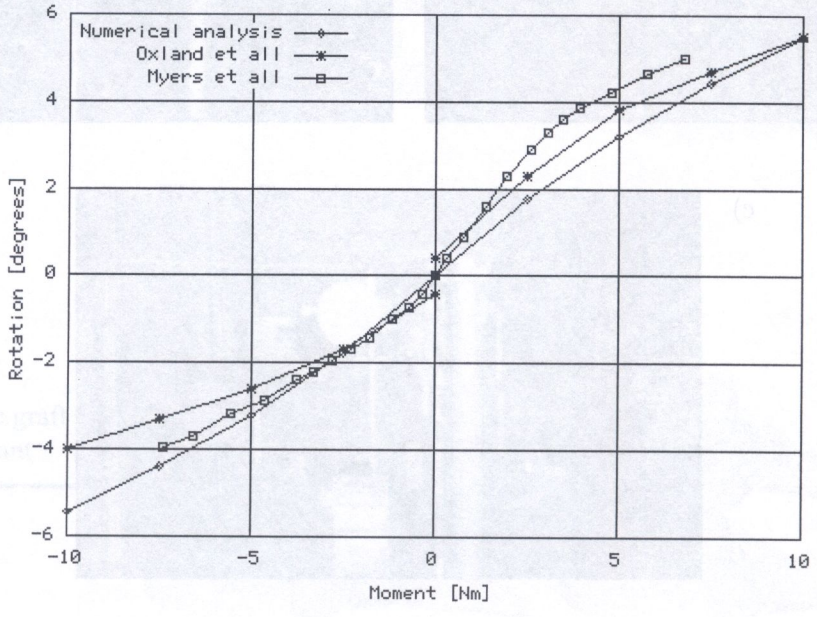

Fig. 9. Moment in flexion–extension versus rotation [8, 17]

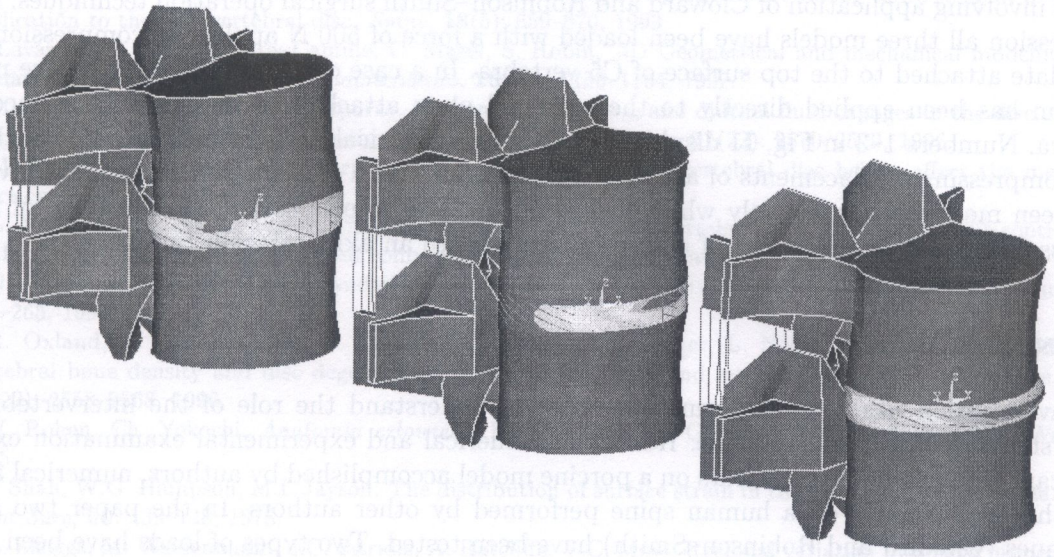

Fig. 10. From extension to flexion-strain variation in the model

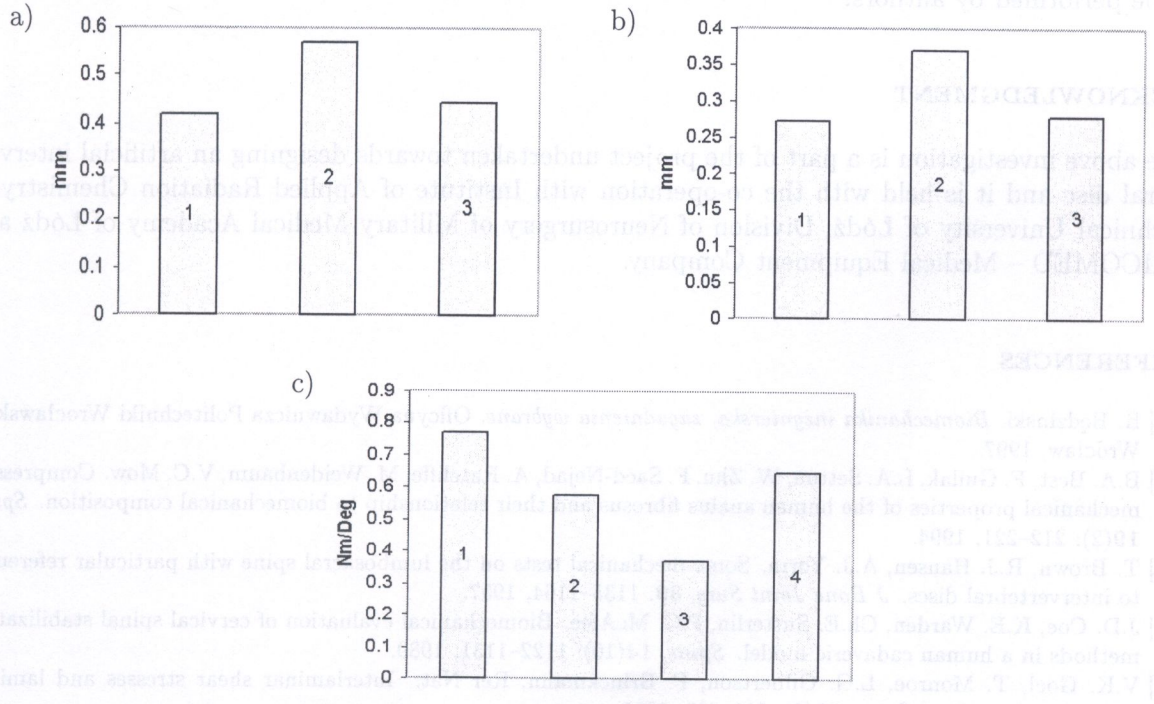

1. Intact spine
2. Cloward operation technique
3. Robinson–Smith operation technique
4. Intact spine – experiment, Coe *et al.* [4]

Fig. 11. a), b) axial compression; c) flexural bending

For cervical spine two types of static loads – axial compression and flexural bending moment have been applied first to a model representing an intact C5–C6 vertebral segment and then to the models involving application of Cloward and Robinson–Smith surgical operation techniques. In axial compression all three models have been loaded with a force of 500 N applied as compression to the rigid plate attached to the top surface of C5 vertebra. In a case of flexural bending a pure moment of 2 Nm has been applied directly to the top rigid plate attached to the superior surface of C5 vertebra. Numbers 1–3 in Fig. 11 display the results of numerical analysis performed by authors. In axial compressing displacements of anterior and posterior nodes of a superior surface of C5 vertebra have been measured respectively while in flexural bending results are shown in a form of flexural stiffness calculated as a quotient of a moment in (Nm) to an axial rotation (in degrees).

9. Conclusion

The investigation has been performed in order to understand the role of the intervertebral disc in the structureof the human spine. Results of numerical and experimental examination exhibited significant similarity of experiments on a porcine model accomplished by authors, numerical analysis and other experiments on a human spine performed by other authors. In the paper two surgical techniques (Cloward and Robinson–Smith) have been tested. Two types of loads have been applied to three models – to an intact C5–C6 spinal segment and then to the vertebras after performing two surgical techniques. Resulting from the numerical analysis one major conclusion can be drawn. In axial compression the largest displacement have been observed after using Cloward technique while flexural tests show that in a contrary to an axial compression model representing Cloward technique seems to be much stiffer then the one of Robinson–Smith. In the paper only preliminary results have been shown. Subsequently numerical investigations will be supported by in-vitro studies which are to be performed by authors.

Acknowledgment

The above investigation is a part of the project undertaken towards designing an artificial intervertebral disc and it is held with the co-operation with Institute of Applied Radiation Chemistry of Technical University of Łódź, Division of Neurosurgery of Military Medical Academy of Łódź and TRICOMED – Medical Equipment Company.

References

[1] R. Będzinski. *Biomechanika inżynierska, zagadnienia wybrane.* Oficyna Wydawnicza Politechniki Wrocławskiej, Wrocław, 1997.

[2] B.A. Best, F. Guilak, L.A. Setton, W. Zhu, F. Saed-Nejad, A. Ratcliffe, M. Weidenbaum, V.C. Mow. Compressive mechanical properties of the human analus fibrosus and their relationship to biomechanical composition. *Spine*, **19**(2): 212–221, 1994.

[3] T. Brown, R.J. Hansen, A.J. Yorra. Some mechanical tests on the lumbosacral spine with particular references to intervertebral discs. *J Bone Joint Surg*, **39**: 1135–1164, 1957.

[4] J.D. Coe, K.E. Warden, Ch.E. Sutterlin, P.C. McAfee. Biomechanical evaluation of cervical spinal stabilization methods in a human cadaveric model. *Spine*, **14**(10): 1122–1131, 1989.

[5] V.K. Goel, T. Monroe, L.G. Gilbertson, P. Brinckmann, Rer Nat. Interlaminar shear stresses and laminae separation in a disc. *Spine*, **20**(6): 689–698, 1995.

[6] D.D. Harrison, T.J. Janik, S.J. Troyanovich, B. Holland. Comparisons of lordotic cervical spine curvatures to a theoretical ideal model of the static sagittal cervical spine. *Spine*, **21**(6): 667–675, 1996.

[7] `http://www.nlm.nih.gov/research/visible/visible_human.html`.

[8] K. Hoshijima, R.W. Nightingale, J.R. Yu, W.J. Richardson, K.D. Harper, H. Yamamoto, B.S. Myers. Strength and stability of posterior lumbar interbody fusion. *Spine*, **22**(11): 1181–1188, 1997.

[9] J.C. Iatridis, M. Weidenbaum, L. Setton, V.C. Mow. Is the nucleus pulposus a solid or a fluid? Mechanical behaviour of the nucleus pulposus of the human lumbar intervertebral disc. *Spine*, **21**(10): 1174–1184, 1996.

[10] M. Krismer, Ch. Heid, W. Rabl. The contribution of anulus fibers to torque resistance. *Spine*, **21**(22): 2551–2557, 1996.

[11] J.P. Laible, D.S. Pflaster, M.H. Krag, B.R. Simon, L.D. Haugh. A poroelastic-swelling finite element model with application to the intervertebral disc. *Spine*, **18**(5): 659–670, 1993.

[12] F. Lavaste, W. Skalli, R. Roy-Camille, C. Mazel, S. Robin. 3D Geometrical and mechanical modeling of the human lumbar spine. *Journal of Biomechanics*, **25**(10): 1153–1164, 1992.

[13] Y.M. Lu, W.C. Hutton, V.M. Gharpuray. Do bending, twisting, and diurnal fluid changes in the disc affect the propensity to prolapse? A viscoelaastic finite element model. *Spine*, **21**(22): 2570–2579, 1996.

[14] Y.M. Lu, W.C. Hutton, V.M. Gharpuray. Can variations in intervertebral disc height affect the mechanical function of the disc?. *Spine*, **21**(19): 2208–2217, 1996.

[15] K.L. Markolf, J.M. Moris. The structural components of the intervertebral disc. A study of their contributions to the ability of the disc to withstand compressive force. *J Bone Joint Surg [Am]*, **56**: 675–687, 1974.

[16] R.N. Natarajan, J.H. Ke, G.B.J. Andersson. A model to study the disc degeneration process. *Spine*, **19**(3): 259–265, 1994.

[17] T.R. Oxland, T. Lund, B. Jost, P. Cripton, K. Lippuner, P. Jaeger, L. Nolte. The relative importance of vertebral bone density and disc degeneration in spinal flexibility and interbody implant performance. *Spine*, **21**(22): 2558–2568, 1996.

[18] J.W. Rohen, Ch. Yokochi. *Anatomia człowieka.* Polish edition by Oficyna Wydawnicza Kalliope, Warszawa, 1995.

[19] J.S. Shah, W.G. Hampson, M.I. Jayson. The distribution of surface strain in the cadaveric lumbar spine. *J Bone Joint Surg*, **60**: 139–148, 1978.

[20] D.L. Skaggs, M. Weidenbaum, J.C. Iatridis, A. Ratcliffe, V.C. Mow. Regional variation in tensile properties and biomechanical composition of the human lumbar analus fibrosus. *Spine*, **19**(12): 1310–1319, 1994.

[21] T.H. Smit, A. Odgaard, E. Schneider. Structure and function of vertebral trabecular bone. *Spine*, **22**(24): 2823–2833, 1997.

[22] G. Smith, R. Robinson. The treatment of certain cervical spine disorders by anterior removal of the intervertebral disc and ineterbody fusion. *J Bone Joint Surg*, **40A**: 607–624, 1958.